J Electroceram (2012) 29:1–7
DOI 10.1007/s10832-012-9726-3

# Effect of discharge power density on the properties of Al and F co-doped ZnO thin films prepared at room temperature

**Boen Houng · Han Bin Chen**

Received: 30 August 2011 / Accepted: 3 April 2012 / Published online: 6 May 2012


**Abstract** ZnO transparent conducting thin films co-doped with aluminium and fluorine (AZO:F) were prepared on glass substrates by RF magnetron sputtering at room temperature. The effect of discharge power density on the microstructure, surface morphology, electrical and optical properties was investigated. From XRD analysis, it was revealed that the intensity of (002) favoured orientation of ZnO films increased with power density from 2.6 to 6.1 W/cm$^2$ and then turned to a randomly orientated structure as power density continuously increased to 7.8 W/cm$^2$. The film prepared at 6.1 W/cm$^2$ showed a better crystallization and microstructure with larger, pyramid-like grains that were approximately 180 nm long and 90 nm wide. As a result, the electrical resistivity of the AZO:F films had a minimum of $4.1\times10^{-4}$ Ωcm. The improvement in the electrical resistivity of AZO:F films was due to the increase in carrier concentration from $8.8\times10^{20}$ to $1.38\times10^{21}$ cm$^{-3}$ and the mobility from 5.8 to 11.8 cm$^2$ V$^{-1}$ s$^{-1}$. The increase in carrier concentration with power density was also found to affect the optical property of the films due to the Moss-Burstein shift.

**Keywords** ZnO thin films · Magnetron sputter · Carrier concentration · Electrical resistivity

## 1 Introduction

Thin film of zinc oxide (ZnO) has been received much attention in the past because of its unique piezoelectric and piezooptic properties that made it suitable for surface acoustic wave devices [1] and optical wave guides [2]. In addition, owing to its direct wide band gap (Eg~3.3 eV), the interest of ZnO in production of green, blue-ultraviolet, and white light-emitting devices [3] is fueled recently. Moreover, doped ZnO thin films as a replacement for indium tin oxide (ITO), are transparent, electrically conductive and have a high refractive index, which has been considered as an excellent candidate for transparent conductive in flat panel display and solar cell devices [4–6]. Doped ZnO thin films have been considered as cost effective replacement of ITO, and may provide numerous benefits like: up to 40 % cost savings, while obtaining even better properties with regards to transparency and electrical conductivity. Another advantage of ZnO is its chemistry stability in the presence of hydrogen plasma which enables for use in the amorphous silicon solar cell fabrication by plasma enhanced chemical vapor deposition [7]. Despite ZnO is naturally an n-type semiconductor, the electrical conductivity of un-doped ZnO is not high enough for practical application. Further reduction of ZnO resistivity can be achieved either by doping it with group III elements, such as B, Al, In and Ga to replace zinc atoms [8], or with group IV elements, such as F, to substitute oxygen atoms [9].

Electrical resistivity, ρ, depends on the carrier concentration (n) and mobility (μ) according to the relationship $1/\rho = ne\mu$, where, e is the electron charge. Obtaining high conductivity in the films is a trade-off between the carrier concentration and mobility because the relationship between the carrier concentration and mobility is governed by the rule $\mu \propto n^{-2/3}$ [10, 11]. The highest reported room temperature Hall mobilities of heavily doped ZnO films are approximately 39 cm$^2$V$^{-1}$ s$^{-1}$, which are limited by ionised impurity scattering [12]. Further increase of the mobility to 200 cm$^2$V$^{-1}$ s$^{-1}$ can be achieved through improving the

B. Houng (✉) · H. B. Chen
Department of Materials Science and Engineering, I-Shou University,
Kaohsiung City 840, Taiwan, Republic of China
e-mail: boyen@mail.isu.edu.tw

crystallinity of the tin films by preparing single crystal or hetero-epitaxial ZnO films [13]. Another way to improve the mobility is to modulate doping through multilayers of heavily and poorly doped semiconducting films [14, 15]. However, data on heavily doped single crystal or epitaxial layers are rare, and the doping relies on advanced deposition techniques and facilities. Therefore, most research efforts have been focused on increasing the effective number of free carriers through impurity doping despite the physical upper limit of carrier concentration at approximately $1.5\times 10^{21}$ $cm^{-3}$ [16]. Single elements, e. g., Al, Ga, In, B and F, are the most commonly used doping agents in ZnO films, and they have been evaluated in a few literatures [8, 9, 11]. However, the resistivity and mobility data are rather scattered and inconsistently reported in the literature. In addition, the optimal chemical and physical properties of current ZnO transparent conducting thin film have not been reached. Nevertheless, new and complex TCO materials are being explored to achieve this goal [17, 18]. For example, co-doping of two elements in ZnO films, such as Al and Ru, Al and Co, Al and Mn, Al and V, and Al and F, has recently been undertaken to optimise the properties of the films for specialised applications [19–23]. Recently, A. Maldonado et. al. and D. C. Altamirano-Juárez et. al. have published a series papers regarding the ZnO films doped with F or/and Al by chemical spraying or dipping coating methods [24–26]. A low resistivity approximately $5\times 10^{-3}$ Ωcm was attained as a result of co-doped with F and Al. In their study, it was found that the combined concentrations of both F and Al dopants should be kept at a small value to achieve low resistivity. Typical values of grain size of the films by such chemical solution deposition techniques are ranged from 10 to 30 μm depending on the annealing condition, which are smaller than physical deposition methods such as magnetron sputtering and pulse laser deposition. In previous works, we prepared the ZnO films co-doped with F and Al elements by magnetron sputtering method. The chemical $AlF_3$ was selected as dopant source to produce n-type semiconducting ZnO films [27]. It provided double doping effects in which the cationic $Al^{+3}$ substitutes the $Zn^{+2}$ ions, and the anionic $F^{-1}$ substitutes $O^{-2}$ ions in the ZnO crystal lattice. The aim of this work is to investigate the properties of ZnO thin films doped with $AlF_3$. The influence of varying sputtering power density on the microstructure, electrical and optical properties of ZnO thin films was presented in this work.

## 2 Experimental procedures

Aluminium and fluorine co-doped ZnO thin films were produced by RF magnetron sputtering on glass substrates (Corning 1373) at room temperature. A mixture of 98 wt % ZnO (Aldrich, 99.99 %) and 2 wt %$AlF_3$ (Aldrich, 99.99 %) powders was sintered as the target for deposition at 1200°C for 4 h. Two center meters square glass substrates were clamped to the grounded electrode, which was maintained at the room temperature. The distance between the target and the substrate was maintained at 8 cm. The vacuum chamber was first evacuated to a pressure of $10^{-6}$ Torr prior to deposition operation, then the sputtering process was carried out at a gas pressure of 3 m mTorr in a pure argon atmosphere. The sputtering time was performed 30 min with sputtering power varying from 50 to 150 W corresponding to discharge power density from 2.6 to 7.8 W/$cm^2$.

An X-ray diffractometer (Panalyical, X'pert Pro) with Cu Kα radiation (λ=0.1542 nm) was used for crystal structure evaluation. The surface microstructure and the morphology of the films were characterised by field emission scanning electron the microscopy (FESEM, Philips, XL-40FEG), atomic force microscopy (AFM, NaniMan NS4 D3100). The composition analysis of the film was conducted through an inducting coupled plasma atomic emission spectroscopy (ICP-AES). The film thickness was measured by scanning electron microscopy measurement. The resistivity was measured with the Van der Pauw method in the four-point probe configuration. The contacts to the samples were made using a high conductivity silver paint. Optical transmittance measurements were carried out in the wavelength range of 300–900 nm using a UV/double-beam spectrophotometer.

## 3 Results and discussion

### 3.1 Microstructure characterisations

The chemical compositions of 2 wt % $AlF_3$ doped ZnO target and thin film are shown in Table 1. The thin film deposited at room temperature showed little variations in chemical compositions from starting target. The composition of F for the thin film was approximately 1.03 wt % which was smaller than that for the target (1.32 wt %). The deposition rate of the films as a function of sputtering power density was shown in Fig. 1. A significant increase of the deposition rate with increasing sputtering discharge power was observed. As the sputtering power density increased from 2.6 to 7.8 W/$cm^2$, the deposition rate of the films increased from 20 to 57 nm/min (corresponding to film thickness of 600 to 1710 nm). This can be explained by the fact that the discharge power was increased, the number of particles generated by sputtering and the probability that these particles arrived at the substrate increased, thus the deposition rate also increased. In addition, the number and kinetic energy of the depositing molecules have been considered as major factors to determine the adatom mobility and formation of the nucleated clusters, which in term

**Table 1** Chemical compositions of the thin film prepared by magnetron sputter and the bulk sample for target measured by ICP-AES

| Chemical compositions | Thin film (wt%) | Target (wt%) |
|---|---|---|
| Zn | 79.49 | 78.96 |
| O | 18.83 | 19.12 |
| AI | 0.65 | 0.62 |
| F | 1.03 | 1.30 |

determine the crystallinity, microstructure and surface morphology of the films [22].

The crystal structure of ZnO films co-doped with Al and F and prepared on glass substrates at room temperature was examined by XRD measurements. Figure 2 shows X-ray diffraction patterns of the AZO:F films produced at room temperatures with varying sputtering power density from 2.6 to 7.8 W/cm$^2$. In all the samples the diffraction peak approximately 34° was observed corresponding to the (002) orientation with a minor (103) peak. This phase was confirmed as ZnO polycrystalline with wurtzite structure and no other crystal phases were found. XRD patterns of these films do not show any appreciable changes from those of pure ZnO films. It was also observed that the (002) peak intensity initially increased with the increase of sputtering power to 6.2 W/cm$^2$, indicating c-axis oriented normal to the substrate. However, it was also noticed that the (002) peak intensity decreased as discharge power was continuously increased. At sputtering power density of 7.8 W/cm$^2$, the film showed a poor crystallization with a random orientated structure.

The effect of the discharge power density on the crystallinity and crystal size of ZnO films was determined according to the Scherrer formula [28]

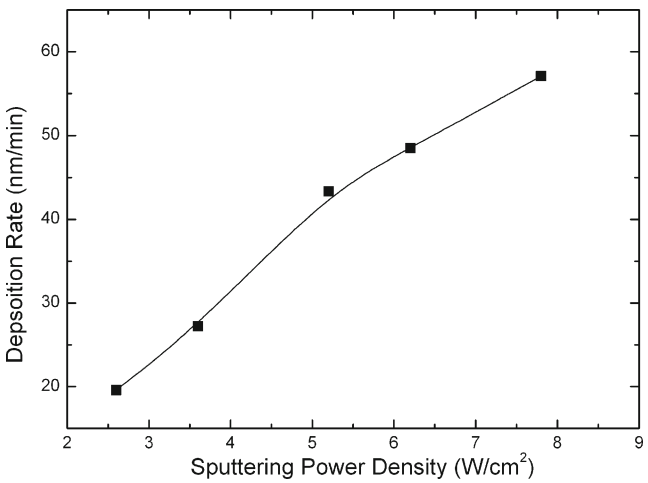


**Fig. 1** Deposition rate of AZO:F films as a function of discharge power density

$$D = \frac{0.94\lambda}{\mathrm{FWHM}\cos\theta} \quad (1)$$

where D is the crystal size of the thin films, θ is the angle of the peak and λ is the wavelength of the X-ray. The full width at half maximum (FWHM) in radian, which is the width of the peak at half the maximum peak intensity, is inversely proportional to the crystal size and is related to the degree of crystallinity in columnar polycrystalline thin films [29]. Figure 3 shows the FWHM values at 2θ of the (102) diffraction peak as a function of discharge power density. The corresponding crystal sizes of the films were also plotted as a function of sputtering power density in Fig. 3. As shown in the figure, the FWHM value was decreased as discharge power density increased and reached to a minimum value at 6.1 W/cm$^2$, which indicated that the crystallinity and crystal size of films were increased as well. After that the FWHM value was then increased, implied that the crystallinity of the films started to degrade as discharge power density increased continuously to 7.8 W/cm$^2$. The dependence of the film crystallinity on the sputtering power can be explained by consideration of the kinetic energies of sputter-ejected species. As applied discharge power was low, few ion bombardments occurred and resulted in a low kinetic energy of the ejected molecules arriving at the grown film. This led to a reduction of adatom diffusion for atomic arrangement and hence tended to form a poor crystal structure. While as sputtering power increased to 7.8 W/cm$^2$, the substrate was subjected to the bombardment at a greater extent, thus this could probably damage the film as a result of high energetic particles impinging on the grown film. It could also produce many crystallography faults in the film and lead to a disorder structure. In addition, the mobility of atoms was greatly increased and resulted in an enhancement of diffusion in the films. Thereby, the films can grow at different crystallographic directions and a more random structure resulted.

The sputtered particles arriving at the substrate can be significantly affect the microstructure and surface morphology of film [30]. The films prepared at room temperature were physically stable and showed very good adherence to the glass substrate. No cracking or peel-off of the films was observed after deposition. FESEM images of the AZO:F films are shown in Fig. 4 with different discharge power densities at room temperature for 30 min. In the case of 2.6 W/cm$^2$, pebble-like grains with an average grain size of approximately 40 nm were observed. This was due to less energetic particles hit on the substrate. Thus, the mobility of atoms deposited on the substrate was small. Consequently, a microstructure contained small grains associated with porosities was formed. As the sputtering power density increased, the large-grain microstructure was developed. The film

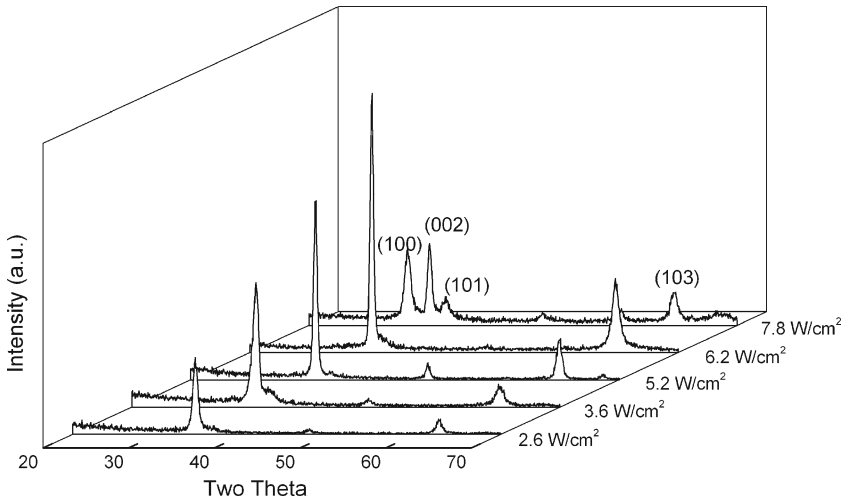


**Fig. 2** XRD of AZO:F films deposited on glass substrate with various discharge power densities

exhibited a surface pyramidal morphology. This surface texturing was a consequence of the nucleation of oriented c-axis grains that grew geometrically and impinged each other laterally [31]. No obvious grain boundary characteristics were observed; the pyramid-like grains were grown to 180 nm long and 90 nm wide at discharge power density of 6.1 W/cm$^2$. As discharge power was increased to 7.8 W/cm$^2$, distinct and irregular grain microstructure was formed; grains with some ridges along the pyramids.

Moreover, the effect of sputtering power on the surface morphology of the films was examined by atomic force microscopy (AFM). It was found that the films sputtered at higher discharge power showed a rougher surface than those sputtered at low discharge power as shown in the AFM images of Fig. 5. The Rms (root mean square) roughness of the film was measured at approximately 4.6 nm for the films sputtered at 2.6 W/cm$^2$ and increased up to 27.8 nm as discharge powers density increased to 7.8 W/cm$^2$. The films deposited at high input powers during sputtering was explored to higher energetic atmosphere that hit the films and resulted in a rougher surface.

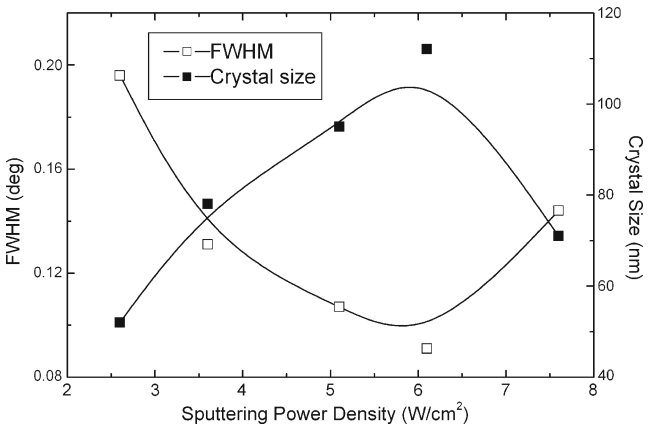


**Fig. 3** FWHM of (0 0 2) diffraction peak and the correspond crystal size of AZO:F films as a function of discharge power density

## 3.2 Electrical and optical properties

The influence of sputtering power density on the electrical resistivity of the AZO:F films deposited on glass for 30 min was plotted in Fig. 6. It was clearly indicated that the electrical resistivity of the films started to decrease from $1.15\times10^{-3}$ Ωcm and reached to a minimum value of $4.1\times10^{-4}$ Ωcm as sputtering power density increasing from 2.6 to 6.1 W/cm$^2$. This accompanied by an increase in the carrier concentration from $8.8\times10^{20}$ to $1.38\times10^{21}$ cm$^{-3}$, while the mobility was also increased from 5.8 to 11.8 cm$^2$V$-1$ s$^{-1}$. The decrease in electrical resistivity was mainly attributed to the enhancement of crystallization of zinc oxide and their dense microstructure with larger grain sizes as seen from the XRD and FESEM results. The denser microstructure contained few pores, which acted as traps for free carriers and barriers for transporting carrier in the film. Hence, the increase in the grain size with less porosity resulted in the reduction of electron scattering and led to the decrease in electrical resistivity. Meanwhile, the films showed an increase in electrical resistivity as sputtering power density continuously increased to 7.8 W/cm$^2$ as a result of the decrease of the mobility, while the electron carrier concentration was reached to a saturated value of approximately $1.35\times10^{21}$ cm$^{-3}$. The higher carrier concentration generated at high sputtering power density may be due to the substitution of more electrically active Al and F atoms into the zinc and oxygen sub-lattice sites, respectively, thereby promoting more free electrons to the conduction band according to the following reaction [32]:

$$AF_3 \xrightarrow{ZnO} Al_{Zn}^{\cdot} + 3F_O^{\cdot} + 4e' \quad (2)$$

where $Al_{Zn}^{\cdot}$ and $F_O^{\cdot}$ represent the aluminum and fluorine ions on zinc and oxygen sites, respectively; e' is an electron in the conduction band. On the other hand, the effect of sputtering power density on the carrier mobility of the thin films can also be seen from Fig. 5. The carrier mobility

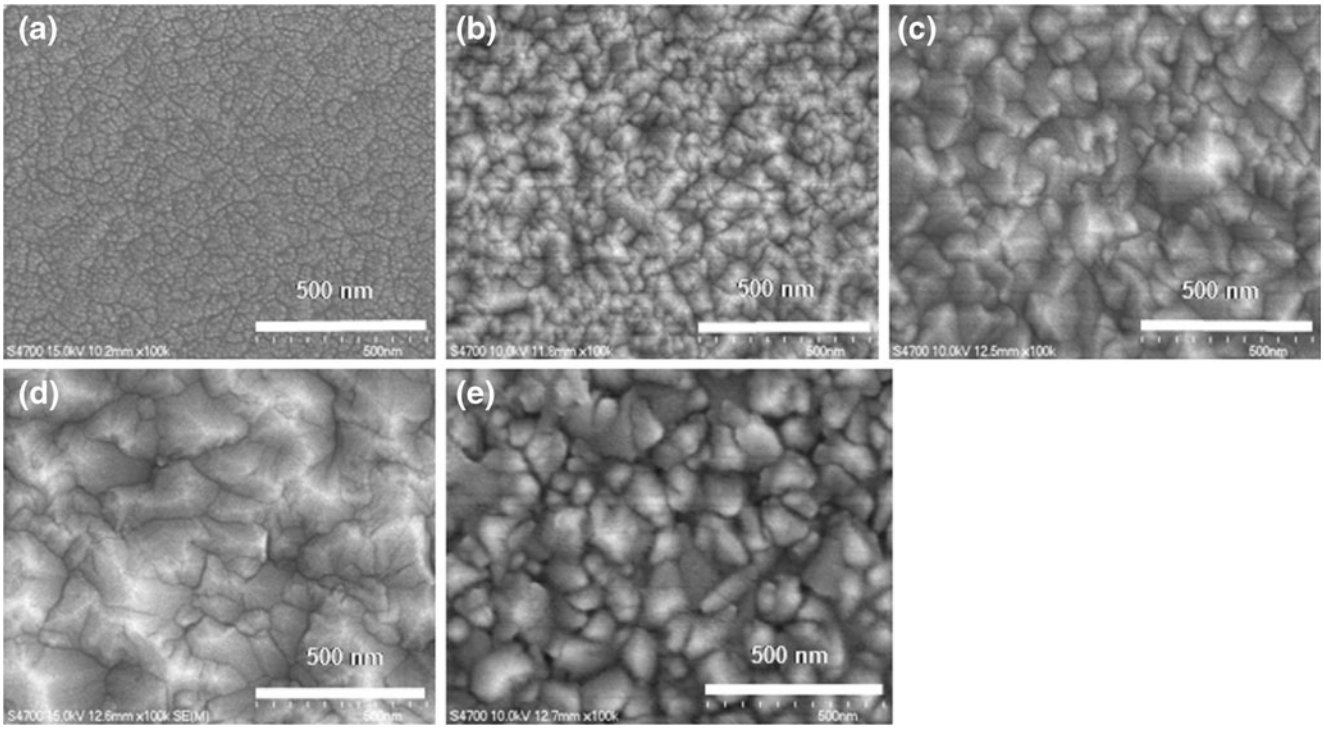


**Fig. 4** FESEM images of AZO:F thin films with discharge power density at (**a**) 2.6, (**b**) 3.6, (**c**) 5.1, (**d**) 6.1, and (**e**) 7.8 W/cm$^2$

increased with sputtering power density from 2.5 to 6.1 W/cm$^2$. This increase in carrier mobility was due to the crystallization enhancement and the increase of grain size in the film. This significantly reduced the grain boundary scattering and raised the carrier mobility. In addition to the grain size, the film surface morphology also has a significant impact on the carrier mobility. We have observed larger surface roughness for the film deposited at sputtering power

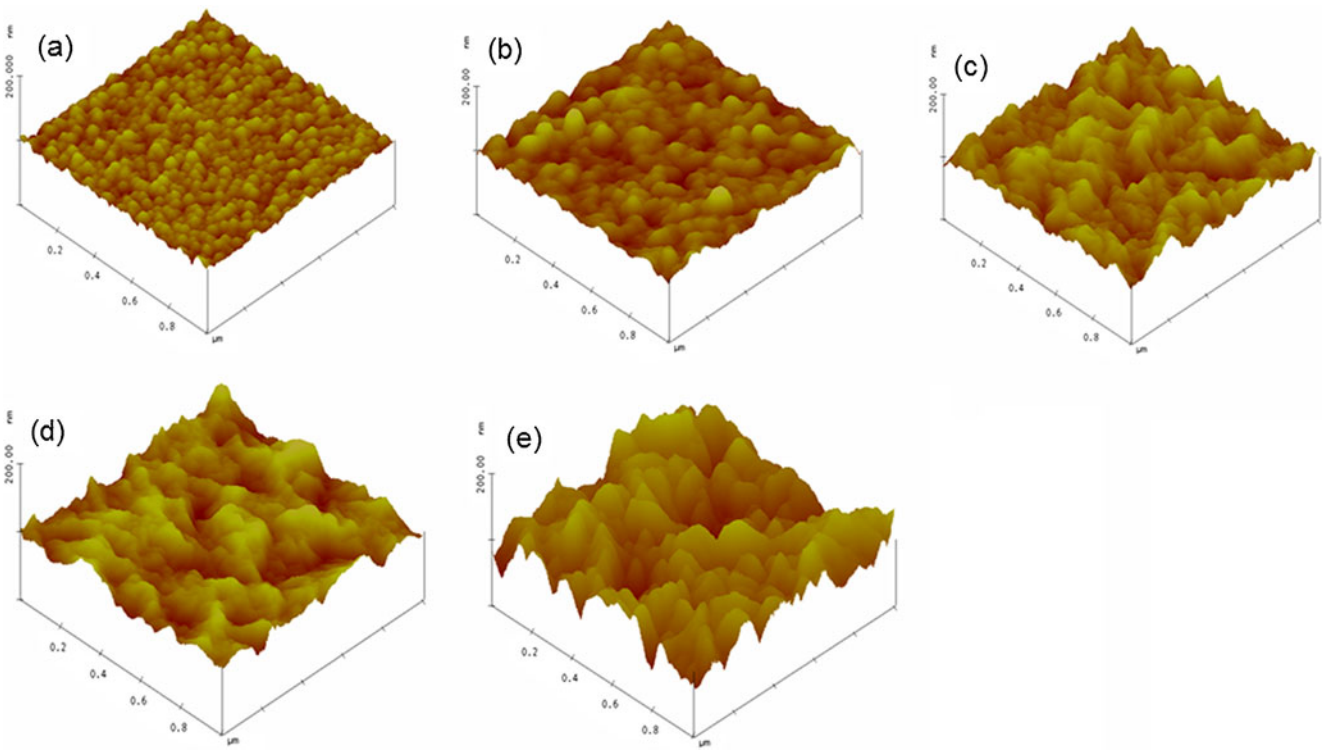


**Fig. 5** AFM images of AZO:F thin films with discharge power density at (**a**) 2.6, (**b**) 3.6, (**c**) 5.1, (**d**) 6.1, and (**e**) 7.8 W/cm$^2$

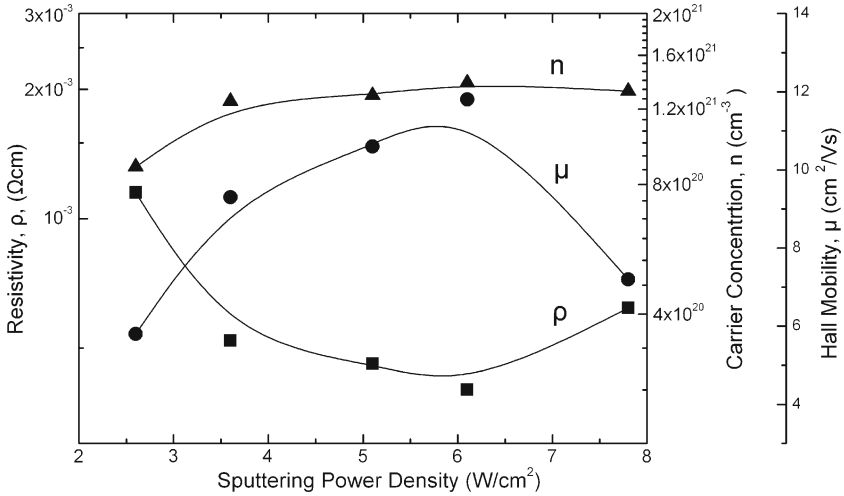


**Fig. 6** Electrical resistivity, carrier concentration and mobility of AZO:F films as a function of discharge power density

density of 7.8 W/cm$^2$ compared to those of lower sputtering power density with an atomic force microscope as mentioned previously. The charge carriers traveling over a rougher surface can be impeded more severely along their mean free path and therefore result in a decrease in mobility.

Figure 7 is an optical transmission spectra of the AZO:F films sputtered at various discharge power densities. The average optical transmission of the samples produced at discharge power density of 2.6 to 7.8 W/cm$^2$ is greater than 80 % in the visible range. However, the film deposited at 7.8 W/cm$^2$ showed the lowest transmission. This variation can be related to film structure. As we have seen from AFM results, the film surface became rougher as the power density was increased and led to more light scatterings and thus a low transmittance in the visible region.

In addition, the absorption edge in transmittance curves was observed a red shift on the wavelength scale for the film with increasing discharge power density. Namely, the threshold of AZO:F films was shifted to shorter wavelengths; thus, the band gap increased due to an increase in the carrier concentration of the film. The optical properties of ZnO films were related to the free carrier absorption and could be expressed by the Drude theory [33]. Using the transmittance and reflectance data, the absorption coefficient ($\alpha$) of the films was calculated according to the following expression:

$$I = I_0 e^{-\alpha d} \tag{3}$$

where I is the intensity of the transmitted light, $I_0$ is the intensity of the incident light and d is the thickness of the film. Using the following relationship, the absorption coefficient data were used to determine the energy gap ($E_g$):

$$\alpha \approx (h\nu - E_g)^{1/2} \tag{4}$$

where hν is the photon energy. In Fig. 8 $\alpha^2$ was plotted against the photon energy of the films shown in Fig. 7. The values of the direct optical band gap, $E_g$, were determined by extrapolating the linear region of the plots to zero absorption. The results suggested that the direct band gap of

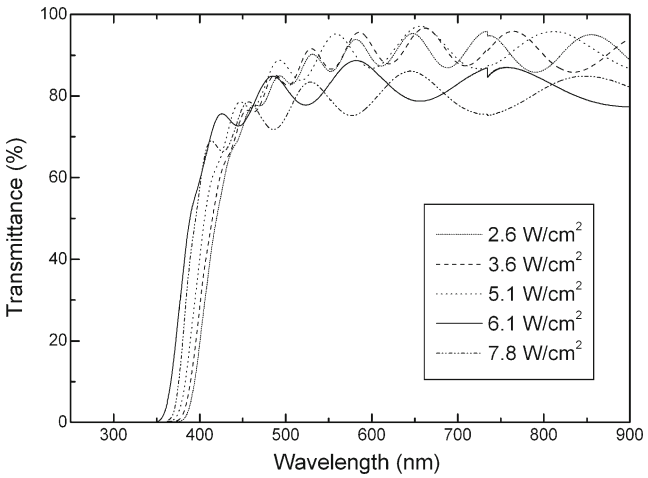


**Fig. 7** Optical transmittance spectra of AZO:F films produced at different discharge power densities

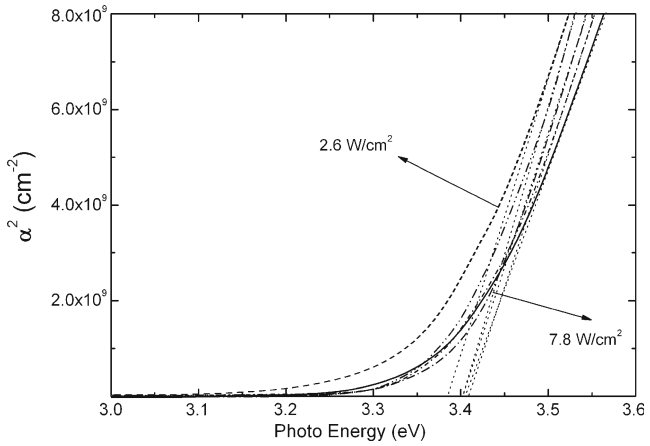


**Fig. 8** Square of the absorption coefficient, $\alpha^2$, plotted against photon energy as a function of discharge power densities corresponding to the samples in Fig. 7

the ZnO film dsposited at 2.6 to 7.8 W/cm$^2$ was 3.382–3.413 eV. The observed widening of the band gap was attributed to a Burstin-Moss shift [34, 35]. According to the Burstin-Moss theory, the lowest states of the conduction band are occupied by free electrons, and valence electrons require extra energy to be excited to higher energy states within the conduction band. Therefore, the optical band gaps of the films prepared at high discharge power were wider than that of the film deposited at low discharge power. Indeed, the optical spectra verified the Hall measurements and suggested that the carrier concentrations for the ZnO films prepared at high discharge power were greater than that for the films produced at low discharge power.

## 4 Conclusions

ZnO thin films co-doped with aluminum and fluorine deposited at sputtering powers density from 2.6 to 7.8 W/cm$^2$ were prepared by RF magnetron sputtering method and their microstructure, electrical and optical properties were examined. It was found that AZO:F thin film showed a trend in the formation of a random crystalline structure as discharge power density increasing to 7.8 W/cm$^2$. The microstructure also revealed a competing growth characteristic of pyramid-like grains with a dimension of 180 nm long and 90 nm width at discharge power density of 6.1 W/cm$^2$. As sputtering power further increased to 7.8 W/cm$^2$, the size of pyramid-like grain was started to decrease and finally became to a loose and irregular shape with few pores microstructure. Nevertheless the film deposited at 6.1 W/cm$^2$ also revealed a minimum value of electrical resistivity about $4.1\times10^{-4}$ Ωcm with carrier concentration of $1.38\times10^{21}$ cm$^{-3}$ and mobility of 11.8 cm$^2$V$^{-1}$ s$^{-1}$. The improvement of electrical conductivity was attributed to a better crystallization and larger grain size. Optical transmittance spectra in visible region of AZO:F films with different discharge power densities are all higher than 80 %, but a lower transmittance for discharge power density at 7.8 W/cm$^2$ due to a rougher surface morphology. The band gaps of the AZO:F films at discharge power density of 2.6 to 7.8 W/cm$^2$ were calculated and the values are within the range from 3.382 to 3.413 eV.

**Acknowledgment** The authors are grateful for the financial support from the National Science Council of Taiwan (GRANT No. 99-2221-E-214-009).

## References

1. C.R. Gorla, N.W. Emanetoglu, S. Liang, W.E. Mayo, Y. Lu, M. Wraback, H. Shen, J. Appl. Phys. **85**, 2595–2602 (1999)
2. M.H. Koch, P.Y. Timbrell, R.N. Lamb, Semicond. Sci. Technol. **10**, 1523–1527 (1995)
3. D.C. Look, D.C. Reynolds, C.W. Litton, R.L. Jones, D.B. Easton, G. Cantwell, Appl. Phys. Lett. **81**, 1830–1833 (2002)
4. G. Hass, J. Heaney, A.R. Toft, Appl. Opt. **18**, 1488–1489 (1975)
5. R. Barber, G. Pryor, E. Reinheimer, SID. Digest of Tech. **28**, 18–23 (1997)
6. G. Sberveglieri, B. Benussi, G. Coccoli, S. Groppelli, P. Nelli, Thin Solid Films **186**, 349–360 (1990)
7. C.G. Granqvist, Thin Solid Films **193/194**, 730–741 (1990)
8. C. Grivas, S. Mailis, L. Boutsikaris, D.S. Gill, N.A. Vainos, P.J. Chandler, Laser Phys. **8**, 326–330 (1998)
9. B.G. Choi, I.H. Kim, D.H. Kim, K.S. Lee, T.S. Lee, B. Cheong, Y.J. Baik, W.M. Kim, J. Eur, Ceram. Soc. **25**, 2161–2165 (2005)
10. R.B.H. Tahar, T. Ban, Y. Ohya, Y. Takahashi, J. Appl. Phys. **83**, 2631–2635 (1998)
11. T. Minami, H. Sato, H. Nanto, S. Takata, Jpn. J. Appl. Phys. **24**, L781–L784 (1985)
12. D.C. Look, D.C. Reynolds, J.R. Sizelove, R.L. Jones, C.W. Litton, G. Cantwell, W.C. Harsch, Solid State Commun. **105**, 399–401 (1998)
13. K. Tominaga, N. Umezu, I. Mori, T. Ushiro, T. Moriga, I. Nakabayashi, Thin Solid Films **334**, 35–39 (1998)
14. I.A. Rauf, Mater. Lett. **18**, 123–127 (1993)
15. K. Ellmer, J. Phys. D. Appl. Phys. **34**, 3097–3108 (2001)
16. T. Minami, Y. Takada, Takata S, T. Kakumu, Thin Solid Films **308**, 13–18 (1997)
17. J.M. Philips, J. Kwo, G.A. Thomas, A.S. Carter, R.J. Cava, S.Y. Hou, J.J. Krajewski, J.H. Marshall, W.F. Peck, D.H. Rapkine, R.B. van Dover, Appl. Phys. Lett. **65**, 115–117 (1994)
18. G.B. Palmer, K.R. Poeppelmeier, Chem. Mater. **9**, 3121–3126 (1997)
19. S. Suzuki, T. Miyata, M. Ishii, T. Minami, Thin Solid Films **434**, 14–19 (2003)
20. H.T. Cao, Z.L. Pei, J. Gong, C. Sun, R.F. Huang, L.S. Wen, Surf. Coat. Tecnnol. **184**, 84 (2004)
21. T. Minami, S. Suzuki, T. Miyata, Thin Solid Films **398–399**, 53–58 (2001)
22. B. Houng, C.S. Hsi, B.Y. Hou, S.L. Fu, J. Alloys Comp. **456**, 64–71 (2008)
23. K. Tominaga, T. Takao, Fukushima, T. Moriga, Nakabayashi, Vacuum **66**, 511–515 (2002)
24. A. Maldonadoa, A. Guillen-Santiagoa, M. de la L. Olveraa, R. Castanedo-Perez, G. Torres-Delgado, Mater. Lett. **59**, 1146–1151 (2005)
25. M. de la L. Olvera, A. Maldonado, R. Asomoza, Sol. Energy Mater. Sol. Cells **73**, 425–433 (2002)
26. D.C. Altamirano-Juárez, G. Torres-Delgado, S. Jiménez-Sandoval, O. Jiménez-Sandoval, R. Castanedo-Pérez, Sol. Energ. Mate. Sol. Cells **82**, 35–43 (2004)
27. B. Houng, H.B. Chen, Ceram. Int. **38**, 801–809 (2011)
28. B. Cullity, Elements of x-ray diffraction. (Addison-Wesley, 1978), 102
29. H. Kim, C.M. Gilmor, J. Appl. Phys. **86**, 6451–6461 (1999)
30. V.T. Cherepin, A.A. Kosyachkov, M.A. Vasilyev, Surf. Sci. **58**, 609–612 (1976)
31. P.M. Verghese, D.R. Clake, J. Mater. Res. **14**, 1039–1045 (1999)
32. D.M. Smyth, The defect chemistry of metal oxides, Oxford University Press, (2000)
33. H.L. Hartnagel, A.L. Dawar, A.K. Jain, C. Jagadish. (Institute of Physics Publishing, Philadelphia 1995)
34. E. Burstein, Phys. Rev. **93**, 63–6332 (1954)
35. T.S. Moss, Proc. Phys. Soc. B. **67**, 775–782 (1964)